We are IntechOpen, the world's leading publisher of Open Access books
Built by scientists, for scientists

6,900
Open access books available

185,000
International authors and editors

200M
Downloads

154
Countries delivered to

Our authors are among the

TOP 1%
most cited scientists

12.2%
Contributors from top 500 universities

CLARIVATE ANALYTICS
BOOK CITATION INDEX
INDEXED

WEB OF SCIENCE™

Selection of our books indexed in the Book Citation Index
in Web of Science™ Core Collection (BKCI)

Interested in publishing with us?
Contact book.department@intechopen.com

Numbers displayed above are based on latest data collected.
For more information visit www.intechopen.com

Temperature Diffusivity Measurement and Nondestructive Testing Requiring No Extensive Sample Preparation and Using Stepwise Point Heating and IR Thermography

Dmitry Yu. Golovin, Alexander G. Divin,
Alexander A. Samodurov, Alexander I. Tyurin
and Yuri I. Golovin

Abstract

This chapter describes a modification to the laser flash method that allows determining temperature diffusivity and nondestructive testing of materials and constructions without cutting samples of predefined geometry. Stepwise local heating of the studied object surface at a small spot around 0.1 mm radius with simultaneous high temporary-spatial resolution infrared (IR) filming of the transient temperature distribution evolution with a thermal camera provides a wide range of possibilities for material characterization and sample testing. In case of isotropic and macroscopic homogeneous materials, the resulting transient temperature distribution is radially symmetric that renders possible to improve temperature measurement accuracy by averaging many pixels of the IR images located at the same distance from the heating spot center. The temperature diffusivity measurement can be conducted either on thin plates or on massive samples. The developed emissivity independent in plain IR thermographic method and mathematical algorithms enable thermal diffusivity measurement for both cases with accuracy around a few per cent for a wide range of materials starting from refractory ceramics to well-conducting metals. To detect defects, the differential algorithm was used. Subtracting averaged radial symmetric temperature distribution from the original one for each frame makes local inhomogeneities in the sample under study clearly discernible. When applied to crack detection in plates, the technique demonstrates good sensitivity to part-through cracks located both at the visible and invisible sides of the studied object.

Keywords: laser stepwise point heating, transient IR thermography, temperature diffusivity measurement, nondestructive testing, crack detection

1. Introduction

Active and passive methods of thermal testing and evaluation have arisen and developed for more than a century [1, 2]. Great progress in thermophysical research has been achieved in the past few decades due to the development of laser and noncontact infrared (IR) thermography technologies [3–5]. The active mode of thermography is most often implemented using optical excitation (stimulation) generated by laser or high-powered halogen lamps with subsequent or simultaneous recording of transient temperature distribution with a high spatial-temporal resolution thermal camera [6–9]. Modern thermographic methods employing mathematical models and thermogram analysis techniques developed in recent years allow extracting a lot of useful information about the state of various objects—from small components of microelectronics [10, 11] to large products [12–15], artworks [16, 17], and engineering structures [14, 18, 19]. They can also be used to conduct nondestructive testing of materials [20–27], determine their thermal physical characteristics (TPC) [28–31], and determine the degree of corrosive damage [32]. Thermography is also used successfully for monitoring natural objects in the environment [33], biomedical research and noninvasive diagnosis of various human diseases [9, 34, 35], and in sports science [36].

For active nondestructive testing (NDT) and TPC measuring, two measurement methodologies are used: steady and transient [3–9, 23, 27–30, 37]. The old steady-state methods (in particular, guarded hot plate (GHP) and heat-flow meter (HFM) [28]) are still used in practice, though they have several disadvantages because the distribution of heat flux should be sufficiently close to the planned asymptotics without significant uncontrolled heat leakage from the measuring cell. These methods require preparation of samples of specific geometry and a long time to achieve steady state.

It greatly complicates the observance of the boundary conditions on the free surfaces of the sample under study adopted in the computation scheme and increases the effect of various drifts on the measurement accuracy. Installations of this type require special measures of thermal insulation and thermal stabilization of the sample, heater, refrigerator, and measuring chain, providing low thermal resistance between the heater, sample, refrigerator, and temperature sensors. Due to the above, installations for the stationary methods are cumbersome, require fairly large samples of strictly defined geometry and thermal conductivity can be measured only within a narrow range.

Transient methods are more diverse. They use various temporal profiles of incoming heat flow such as Dirac delta function, step or periodic ones [18, 23, 27, 28, 38]. The latter mode is used by thermal wave interferometry (TWI) technique, which opens additional possibilities related to synchronous signal detection referred to as lock-in technique like accuracy improvement, reduction of drift impact, and gathering information from two independent channels, namely signal amplitude and phase [38–40]. However, due to the necessity for oscillations to be close to asymptotic, this method exhibits some of the abovementioned drawbacks of stationary methods. Another disadvantage of this technique is the high cost of the required hardware.

Among nonharmonic transient techniques of thermal stimulation, laser flash technique (LFT) proposed back in 1961 by Parker et al. [41] is the most widely used up to date. It can be easily adopted for testing plate samples of homogeneous [42], anisotropic [43, 44], porous [45], translucent [46] solids as well as liquids [47–52]. LFT is supported by commercially available equipment [53, 54] operating according to established standards [55–57].

Further advances in LFT result in variants employing thermal wave propagation not only in normal direction as in classic LFT [41], but also in plane techniques [44, 58–62]. It uses point heating to implement the radial diverging thermal wave technique for immobile objects [44, 58–61] and for moving ones [62]. Heating from ring-shaped area in the radial converging thermal wave technique provides better signal/noise ratio and reduces overheating in the irradiated area [63–67]. These variations of LFT allow TPC evaluation and NDT in case of one-side access to the object but use short pulse heating.

The conventional laser flash technique and appropriate equipment has a number of undeniable advantages including high accuracy and good reproducibility of measurements, short testing times ($\sim$1 s), optional control over surrounding gas composition, and temperature in wide range (from -120 to 2800°C). However, it has several immanent drawbacks. LFT testing requires specifically prepared samples of the certain geometry. Usually, it is a disk with a diameter of 12–25 mm and thickness $\sim$1 mm. The experiments are costly and time-consuming, and they require two-side access to the sample. This prevents using the method on massive or unprepared samples as well as on finished goods in operation or the ones that can be accessed from one side only.

So, the purpose of the work is development of all-round express technique for temperature diffusivity (TD) *a* measurement in various materials and objects requiring no extensive sample preparation as well as technique for detecting various inhomogeneities and defects in the material. The original algorithms and software were designed and implemented.

2. Methods and materials

The proposed method [68] is based upon thermal imaging of transient temperature field induced by local spot, further referred to as point heating. Original algorithms and software are used for processing IR images recorded by a thermal camera.

Thermal cameras are used in various applications [2, 3, 21, 23, 24] and have many advantages for recording temperature distribution evolution in a studied object. Cameras have a number of advantages over local temperature sensors such as thermocouple elements or thermistors, beside their evident ability to register temperature in a great number of points remotely and simultaneously. High accuracy of data spatial localization, no problems related to thermal inertia, additional thermal capacity, heat sink, and boundary thermal resistance of the gauge should be mentioned as the most prominent ones.

Meanwhile, it should be noted that the lack of accurate information concerning optical absorption and radiation coefficients of the studied object and their variations along the surface render precise measurement of absolute temperatures and heat fluxes in an object difficult in case of laser heating and IR camera recording. But, similar to LFT, the proposed technique requires no absolute values of temperature because the nature of temperature diffusivity a is determined by characteristic length r and time t of thermal wave propagation from hot spot as could be seen from its physical meaning, m^2/s units and dimensionless Fourier similarity criterion $F_0 = at/r^2$. The only important reservation concerns the uniformity of the coefficient between the absolute temperature and acquired signal all over the studied surface. By the way, it is also true for classic LFT that determines the time of reaching the half of temperature maximal value at the back side of the sample of known thickness but not absolute value of the temperature itself.

The proposed approach utilizes step-like temporal profile of point local heating of the surface by laser beam with Gauss radius r_0 = 0.1–0.3 mm and simultaneous filming of transient temperature field induced by this heating at the object surface by an IR camera. In our experiments, laser heating has constant power during all testing time (step-heating thermography) like [69–72] whereas classic LFT uses short pulse heating [44, 58–66]. It significantly reduced the temperature in the hot spot, while increasing it in the surrounding inspected area and lowering requirements to laser output power. The following computer processing of radially symmetric thermal images using the proposed models and algorithms allows determining the value of a in homogeneous materials and detecting and characterizing inhomogeneities and defects owing to local divergence of temperature distribution from axial symmetry. Two variants of the method are considered in the paper namely one for bulk and the other for thin plate objects. They are related to standard LFT but do not require extensive sample preparation.

Verification of the described approach to measurement of a has been done for a number of materials (see **Table 1**) with significantly different thermal and optical properties. A 2-mm-thick square steel plate of 100×100 mm was used as a sample. Its TD was determined using a 2D model of thermal wave. All other samples were massive disks with diameter > 30 mm and height > 25 mm. They were studied using a 3D model.

A solid-state Nd:YAG laser unit LSR445CP-FC-10 W with diode excitation, maximal output power of 12 W, 445 nm wavelength, and controllable intensity was used as a heater. Digital IR filming of the object surface was done using an FLIR A35sc thermal camera having 320×256 pixels matrix of VO_x bolometers with maximal sensitivity in 7.5–13 mkm range, angular resolution 2.78 mrad, sensitivity $\sim$0.05°C in the range from -20°C to $+550$°C and frame rate up to 60 Hz. Individual frames like the ones shown in **Figure 1** were converted to two-dimensional temperature maps. To suppress signal inhomogeneities originating from differences in

Material	Composition	Short name
Dense stabilized ceramics ZrO_2:MgO	ZrO_2 (98%). MgO (2%).	Ceramics
Composite based on phenol-formaldehyde polymer	Phenol-formaldehyde polymer (50%) + mica (15%), carbon black (15%), kaolin (10%), talc (5%), and cellulose (5%).	Composite
Cured rubber	Synthetic rubber (60%), carbon black (30%), ZnO (8.5%), and S (1.5%).	Rubber
Teflon (white)	Tetrafluoroethylene	Teflon-w
Teflon (black)	Tetrafluoroethylene + carbon black (40%)	Teflon-b
Gypsum	$CaSO_4 \cdot 2H_2O$ (at least 90%); SiO_2, Al_2O_3, Fe_2O_3, and other (no more than 10%).	Gypsum
Mild carbon steel "Steel 40X" (Analogue of mild carbon steel AISI 5140)	C (0.36–0.44%), Si (0.17–0.37%), Mn (0.5–0.8%), Ni ($\leq$0.3%), Cr (0.8–1.1%), the rest is Fe	Steel

All per cents are mass ones.
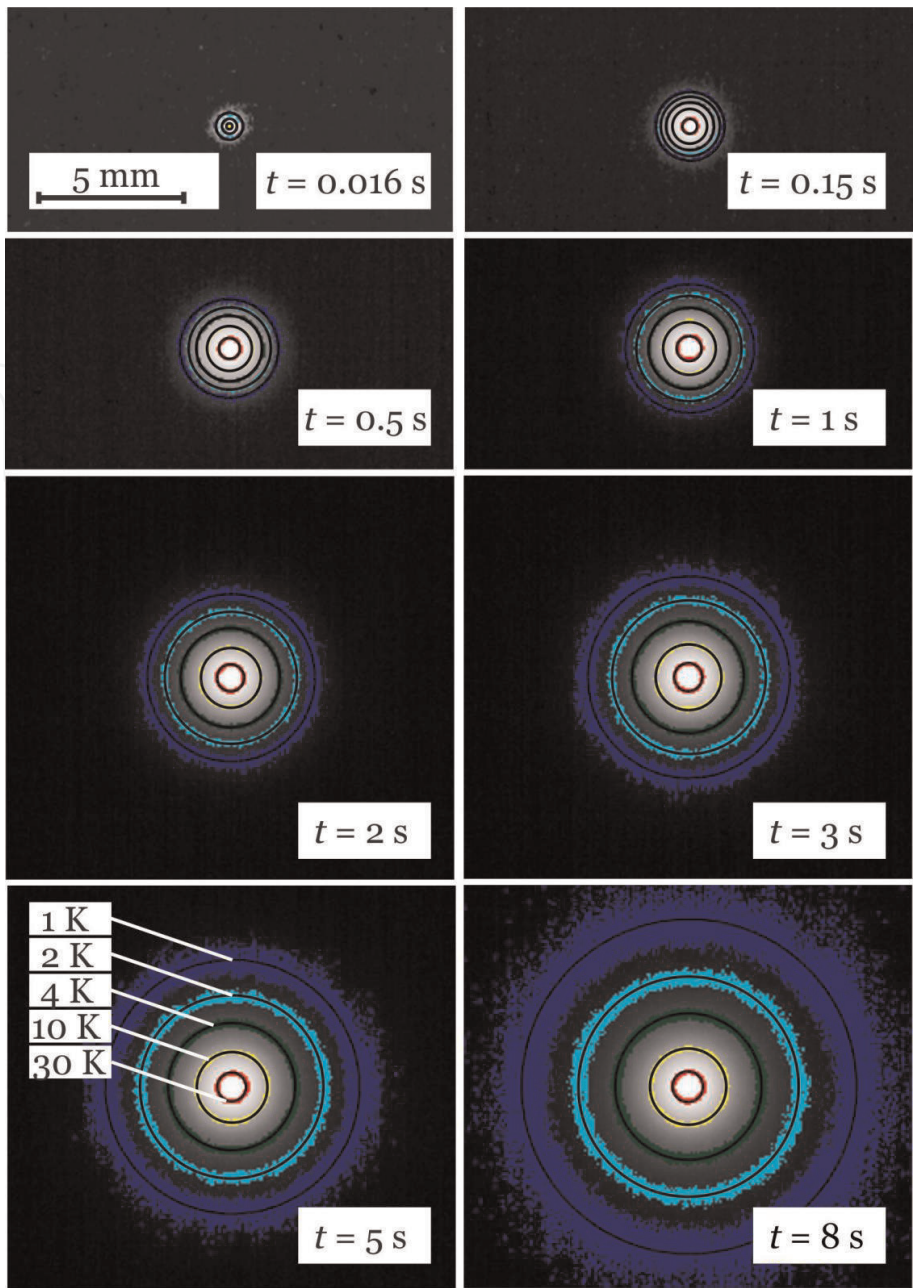
Table 1.
Tested materials.

Figure 1.
Certain frames of IR film with added isotherms showing thermal wave propagation resulting from local heating of a ceramic sample. Colored rings correspond to 1 ± 0.25 K, 2 ± 0.25 K, 4 ± 0.5 K, 10 ± 1 K, and 30 ± 5 K.

local surface emissivity, the initial temperature T_0 before the heating onset has been subtracted from temperature T_h recorded during heating for every pixel. From now on, the temperature excess $T = T_h - T_0$ is the signal to be analyzed. The next step is determining position of effective center of the heating and averaging the values of T over the angle φ (see **Figure 2**) for each given distance r from the center to reduce noise, impacts of inhomogeneities, etc. Averaging T over φ is executed in ring-shaped areas limited by radii $r - \Delta r$ and $r + \Delta r$, where Δr is defined by image pixels size and is about 2–10% of r. Usually, $\varphi = 360°$ in TD measurements, and in NTD testing, $\varphi < 360°$ to exclude the area with suspected defects.

The detailed step-by-step raw data processing algorithm is as follows:

1. converting native data format of recorded film in a series of two-dimensional arrays of temperatures;

Figure 2.
Raw data processing scheme. Averaging the temperatures from a set of pixels located at the same distance r in a fragment of last frame from **Figure 1.**

2. determining the time of heating onset (in case of the lack of hardware synchronization);

3. averaging each pixel over time before this moment and forming the base frame;

4. pixel-by-pixel subtraction of this base frame from each following frame to suppress the impact of local inhomogeneities of studied surface optical properties;

5. determining the effective center of the heating;

6. averaging temperatures of all the pixels located at the same distance from the heating center. In case of NDT, one needs to search and exclude the areas significantly differing from the mean value to avoid artifacts. The temperatures averaged in the above procedure form the target radial temperature distribution $T(r)$ for the frame. On processing all the frames, one gets $T(r, t)$ distribution; and

7. approximating experimental radial temperature distribution $T(r)$ by function (2) using the Nelder-Mead method [15] in case of 3D model or using linear regression in appropriate coordinates for 2D model. Spatial and temporal limits of the area for data to be approximated are determined by the assumptions made in building model and approximating function. From below, the data related to $t < 3t^*$ and $r < 2r_0$ are ignored, and from above, the areas are restricted by a stronger limit of (a) T should be above 1/10 of maximal accepted value and (b) T should exceed tripled root-mean-square value of the noise.

Distributions $T(r, t)$ obtained for two macroscopically homogeneous defect-free samples using 2D and 3D techniques as described above are presented in **Figure 3**. It should be noted that for thin plates tested in 2D mode, IR camera can be located either at the same side or at the opposite side relative to the incident laser beam (see inset in **Figure 3**). It does not matter principally, but slightly affects details of implementation.
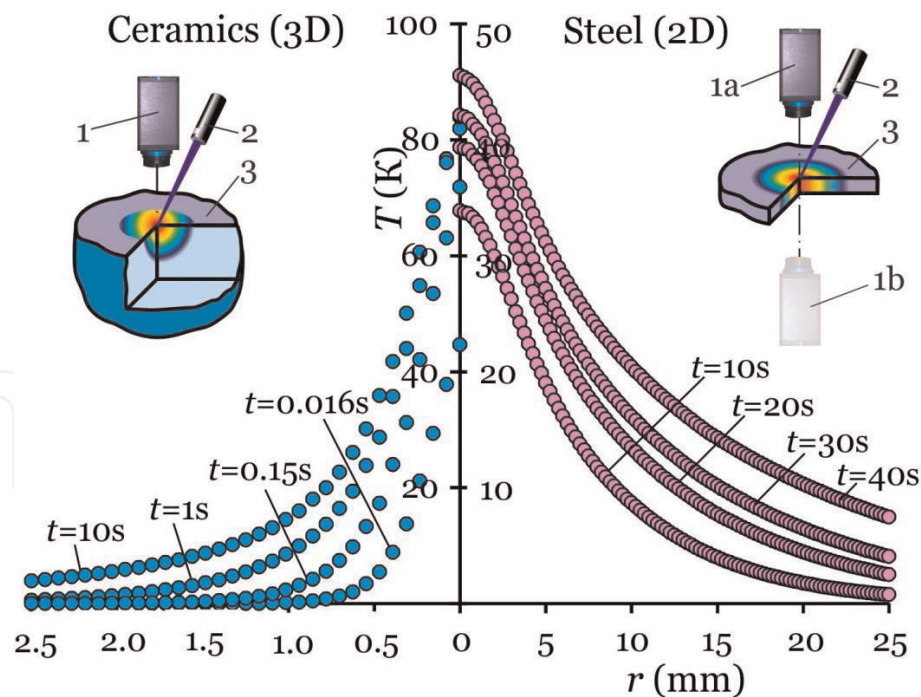
Figure 3.
Experimental radial dependencies of temperature excess T in massive ceramic (3D) and steel plate with a thickness of δ = 2 mm (2D) samples at different times t since the heating onset. r is the distance to the heating center. 1—IR camera; 1a u 1b—two variants of camera positions; 2—laser; and 3—sample. Insets show the experiment layout and color-coded temperature distributions near the heating center.

3. Thermal diffusivity measuring: 3D model

Point heating at the surface of a massive isotropic and homogeneous sample induces radially symmetric spherical thermal wave in the semi-infinite space. The measurement duration τ should be at least an order of magnitude higher that characteristic time $\tau_F = (r_0)^2/a$ for a given material and Gaussian radius of heating spot r_0, so that the thermal wave has sufficient time to propagate to the distance $r > (3-5)r_0$. For $r_0 \sim 0.1$ mm, minimal value of τ is usually below a second for all materials, and for $r_0 \sim 0.3$ mm, it is tenths of a second for metals, a few seconds for ceramics and the like, and up to a few tens of seconds for materials with the lowest values of TD coefficient like highly porous medias and some polymers. Provided condition $\tau \gg \tau_F$ is met, particularly radial distribution of energy in incident beam becomes insignificant at the distances from the heating center $r > (2-3) r_0$, and temperature distribution in homogeneous semispace can be considered spherically symmetric up to the times limited only by thermal wave approaching the boundaries of the heated object. For the above values of temperatures, times and distances, the heat exchange at the free surface can definitely be neglected.

Even for isotropic homogeneous materials without temperature dependence of TPC in adiabatic approximation, that is neglecting heat exchange at the surface, and for energy of incident laser beam transferred to the sample not just at the surface but in a sphere with radius R, so that the heat flux through it is uniform and Q in total, precise solution of Fourier heat transfer equation is quite complex and hardly applicable for experimental data analysis [73]:

$$T(r,t) = (Q/2\pi\lambda r)\left[\mathrm{erfc}\left((r-R)/2(at)^{1/2}\right) - \exp\left[(r-R)/R - at/R^2\right]\right.$$
$$\left. \mathrm{erfc}\left[(r-R)/2(at)^{1/2} + (at)^{1/2}/R\right]\right] \tag{1}$$

where $\mathrm{erfc}(x) = \frac{2}{\sqrt{\pi}} \int_x^\infty e^{-y^2} dy$ is the complementary error function and λ is the material thermal conductivity. Besides, any accurate solution as in Eq. (1) depends upon poorly known energy distribution in the heating spot and optical properties of material such as absorption and stray light factors. However, for $r \gg r_0$ and $t \gg t^* = r_0^2/a$, the temperature distribution $T(r, t)$ can be approximated with accuracy around 1% by function.

$$T(r,t) = Br^{-1}\mathrm{erfc}\left[0.5(r{-}r_0)(at)^{-1/2}\right] \qquad (2)$$

where B is some constant depending upon supplied energy, r_0 and λ.

As could be seen from Eq. (2), temperature distribution approaches asymptotic $1/r$ in time t, determined by the value of a. To obtain the value of a from experimental data manually, it is rational to redraw distribution $T(r, t)$ in $(T_r, (r - r_0)t^{-1/2})$ coordinates and then approximate if with a function $y = D \cdot \mathrm{erfc}(A \cdot x)$, varying only scales of the axes. As follows from Eq. (2), the value of $A = 0.5a^{-1/2}$ found in this way allows determining $a = (4A^2)^{-1}$. In computer-aided analysis, experimental distributions have been fitted using Nelder-Mead method minimizing sum of squared discrepancies either directly using the function Eq. (2) or in the coordinates described above. Both variants give the results of similar quality. In real experiments, accuracy of T recording deteriorates with growing r due to finite temperature resolution of the camera and growing role of noises of various nature, so that the reasonable testing duration lies in the range $3\tau_F \lesssim \tau \lesssim 10\tau_F$. Raw experimental data processed as described above is shown in **Figure 4**.

Values of a calculated as described above for each of eight individual tests, standard deviation δa of the sampling within each test, averaged value a_8, and standard value a^* for each of the tested materials are presented in **Table 2**.
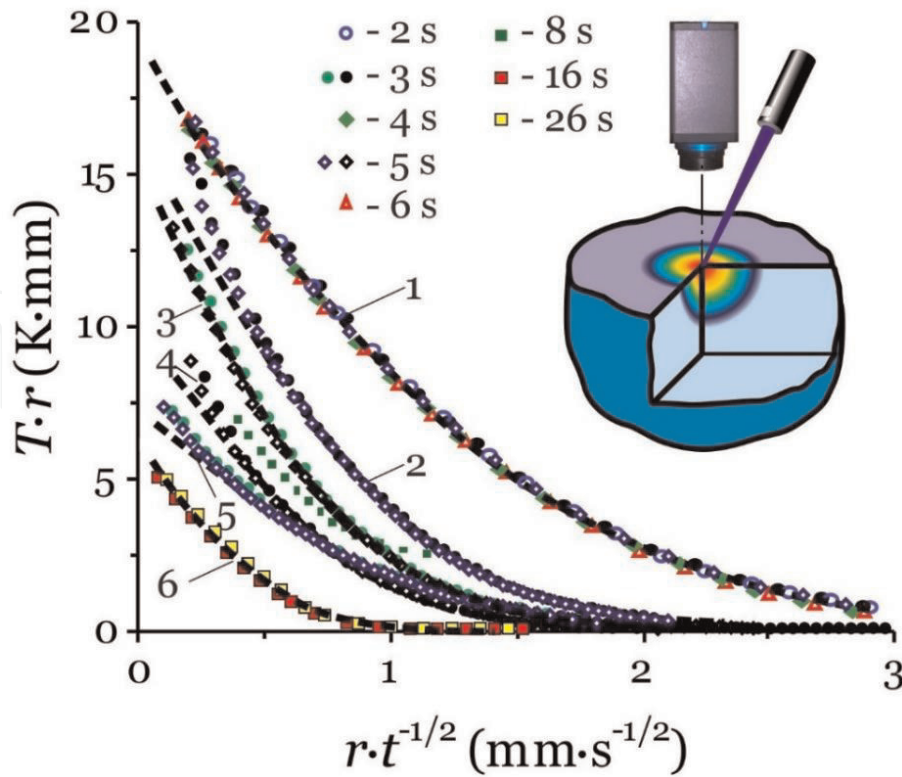

Figure 4.
Experimental temperature dependencies on radius and time in coordinates. $T_r = f[(r - r_o)t^{-1/2}]$ are shown by dots and computation results according to the described model shown by dashed curves for the following materials: 1—ceramics, 2—teflon-b, 3—composite, 4—rubber, 5—gypsum, and 6—teflon-w. The dot shapes correspond to acquisition time. Inset outlines the experimental setup.

Material	Measured and standard values of a (mm²/s)	Test number							
		1	2	3	4	5	6	7	8
Ceramics	a	1.041	1.010	1.033	1.091	1.076	1.046	1.001	1.040
	δa	0.011	0.018	0.017	0.026	0.012	0.015	0.019	0.010
	a_8	1.042 ± 0.016							
	a^*	1.120 ± 0.096							
Composite	a	0.238	0.244	0.237	0.240	0.227	0.233	0.237	0.238
	δa	0.014	0.019	0.011	0.044	0.010	0.009	0.017	0.005
	a_8	0.237 ± 0.016							
	a^*	0.276 ± 0.033							
Rubber	a	0.239	0.268	0.240	0.239	0.246	0.265	0.243	0.255
	δa	0.039	0.008	0.017	0.019	0.015	0.017	0.015	0.015
	a_8	0.249 ± 0.018							
	a^*	0.249 ± 0.032							
Teflon-w	a	0.119	0.114	0.115	0.129	0.127	0.113	0.123	0.128
	δa	0.006	0.005	0.004	0.005	0.007	0.004	0.007	0.007
	a_8	0.120 ± 0.005							
	a^{**}	0.118 ± 0.003							
Teflon-b	a	0.323	0.319	0.355	0.333	0.336	0.336	0.327	0.326
	δa	0.006	0.008	0.009	0.035	0.013	0.017	0.016	0.015
	a_8	0.332 ± 0.015							
	a^*	0.389 ± 0.055							
Gypsum	a	0.432	0.430	0.391	0.422	0.434	0.365	0.465	0.437
	δa	0.024	0.013	0.026	0.012	0.041	0.019	0.030	*0.039*
	a_8	0.422 ± 0.026							
	a^{**}	0.427 ± 0.007							

*Value obtained using standard HFM technique [28].
**Standard reference value [74].

Table 2.
Measured and reference values of a *for tested materials.*

Figure 5 shows elementary values of a; i.e., each dot corresponds to one frame of the film as a function of time t since the onset of heating for a number of tests of each material. As could be seen, the proposed technique and model produce very close values of a at a wide range of t depicted by oval curves. It allows collecting large statistics in one test to reduce measurement uncertainty originated from various random factors by averaging the set. Some variations in a value calculated based on different tests of the same material but with differing positions of heating center can be accounted for real inhomogeneity of material TPC.

To determine thermophysical properties of the same materials independently, standard steady-state HFM [28] for measuring thermal conductivity λ_{st} of $\sim$1-mm thin plates with known passed heat flux has been used. Temperature diffusivity coefficient $a^* = \lambda_{st}/\rho c_p$ has been calculated for each material based upon independent measurements of density ρ and specific heat capacity c_p. As followed from **Table 2**, values of a, determined using the proposed technique, and the values of a^*, obtained
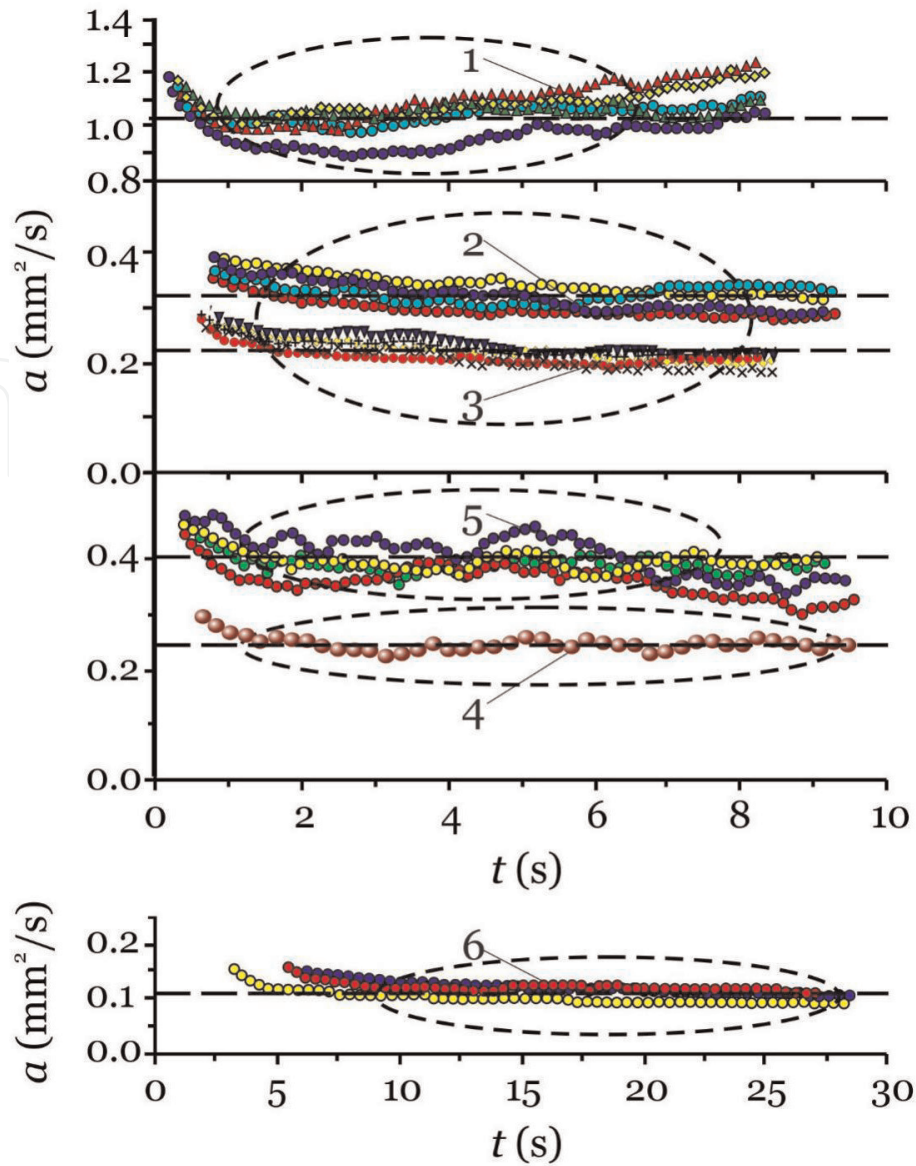
Figure 5.
Dependence of temperature diffusivity a on the time t passed since the heating onset. Dots correspond to experimental data and dashed lines show average value. 1—ceramics; 2—teflon-b; 3—composite; 4—rubber; 5—gypsum; and 6—teflon-w.

using standard steady-state technique, coincide within the stated inaccuracies of both the methods. For some of the materials, standard values a^{**} obtained from reference tables are shown instead of measured value a^{*}.

As could be seen from **Figure 5** and **Table 2**, relative random errors of a amount to several per cent. Systematic errors are generally of the same level. Origins of the latter ones are numerous, and the largest impact occurs from image scaling and optical aberrations of the camera, nonadiabatic heating growing with testing time, temperature dependence of TPC, especially in case of plastics, and transparency and reflectivity of studied material. Suppressing them is the objective of the next stage of the refinement technique.

As for effects of temperature dependence of TPC, they are determined by the following factors. Maximal temperature excess at the surface of a given material depends upon heat flux density and beam focusing radius. In all cases, it does not exceed a few tens of °C and several °C in the measurement area, so that the obtained results correspond to the temperature of environment in the first approximation. To reduce the possible impact of TPC temperature dependence on the measurement of a, one should either reduce temperature gradients in the measurement area or the

area dimensions provided the gradients are the same. The former is achieved due to constant heating unlike instant heating in LFT. To reduce it further, which could be desirable for temperature-sensitive materials, one should increase heating spot radius r_0 and/or decrease energy density in an incident beam, but the former requires increasing measurement time τ, while the latter leads to reduction in signal/noise ratio, and both ways result in growing inaccuracies.

4. Thermal diffusivity measuring: 2D model

For thin plates, films or shells of highly conductive materials with thickness lying in the range $\delta \sim 0.1$–3 mm, it is possible to use similar technique, but forming cylinder thermal wave instead of spherical one. This approach has been widely used since the 1930s, it is standardized for measuring TPC of gaseous, liquid, solid, and noncoherent materials and is referred to as linear heat source or transient hot-wire (THW) technique [28, 75–79].

The proposed technique differs from the THW in heating zone geometry. In the standard technique, a cylinder thermal wave is induced by a linear heat source with the length much higher than thermal wave radius, while the proposed technique utilizes a point heat source at the surface of the plate, in which thickness is much less than the thermal wave radius. In both cases, temperature distribution is the same at distances several times higher than the maximal characteristic length of the problem, that is the highest of heating area size and plate thickness, and can be described by the following expression [73].

$$T(r,t) = (Q/4\pi\lambda\delta)\ln\left(4at/Cr^2\right) + O\left(r_0^2/at\right) \tag{3}$$

where Q is the total power transferred to the plate, r_0 is the heating area radius, $\ln C = \gamma \approx 0.5772$ is the Euler constant, and $O(x)$ is some function limited by its argument multiplied at some finite constant. The second term in Eq. (3) may be neglected in practice for times high enough so that $t \gg \tau_F$. Unlike the case of a massive object and spherical thermal wave, the distribution $T(r, t)$ in this case does not approach to some steady asymptotic but keeps growing logarithmically with time. Provided heating power and testing time remain unchanged, the temperature reaches much higher values than in a massive object. It allows reaching significantly higher relative precision of TD measurements with the same power of laser beam or reducing the latter to decrease object overheating while keeping measurement accuracy.

Linear regression $y = d \cdot (x - g)$ in $(\ln(r \cdot t^{-1/2}), T)$ coordinates is used to calculate TD from the experimental data. As follows from Eq. (3), TD and the value of g are related as $a = \exp(2g - \gamma)/4$. Experiments were carried out on a low carbon steel plate with dimensions $100 \times 100 \times 2$ mm. As a result of the processing of each frame of IR film, radial dependence $T(r)$ at different moments of time t since the heating onset has been found (see **Figures 2** and **6**) and then the values of a for each frame is found. Averaging a over several hundreds of frames of each film, one can obtain the mean value of a for each individual test. Statistical processing of 10 such mean values of a obtained in 10 different films results in $a = (12.54 \pm 0.27)$ mm²/s (**Figure 7**). It coincides with the standard value of TD for low carbon steels, and relative root mean square of the set is as low as 2%. Using the above value of a, standard values for density $\rho = 7870$ kg/m³ and specific heat capacity $c_p = 486$ J/(kg. K) for low carbon steel and relation $\lambda = a\rho c_p$, one can find the value of $\lambda = 48.0$ W/(m.K).
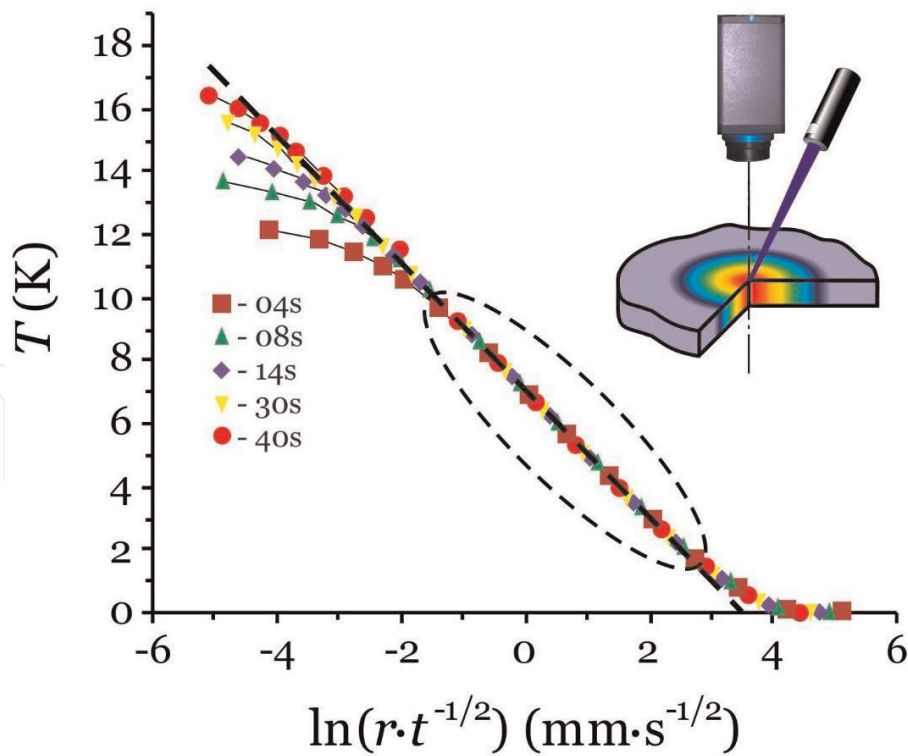
Figure 6.
Experimental data (dots) and their linear regression (dashed line) in 2D testing of a low carbon steel plate. Inset shows the experimental setup.
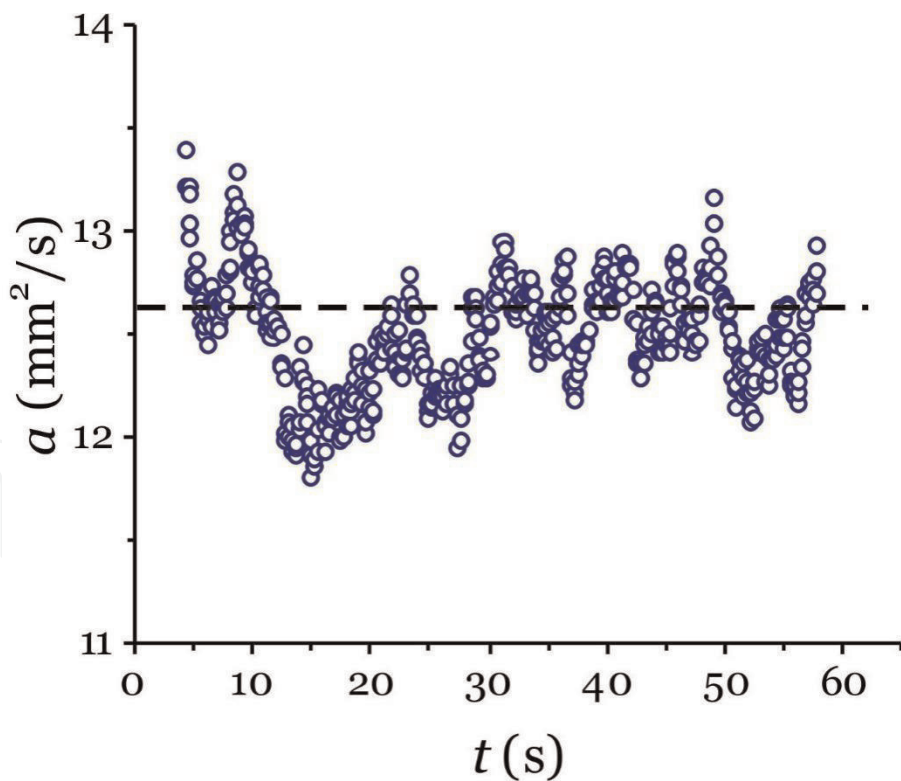

Figure 7.
Dependence of elementary values of temperature diffusivity a over time t passed since the heating onset for a low carbon steel sample. Dots represent experimental results and dashed line shows an average value.

5. Discussion of thermal diffusivity measuring

The two described variations of the presented technique complement each other. Spherical wave mode is applicable to any sample having dimension large

enough (minimally $10r_0$), and testing duration is quite short, namely around a few tens of Fourier time for hot spot size. Typically, testing takes from a fraction of a second to a few seconds. Cylinder wave mode works better on highly conductive materials, but takes more time (usually tens of seconds) and imposes restrictions on sample thickness δ. From below, it is limited by growing impact of heat transfer through free surfaces, which is characterized by the ratio of the energy that left the sample through the surfaces to the stored energy at the column perpendicular to the plate plane $\alpha\tau/\rho c_p\delta$, where α is the total surface heat transfer coefficient including both convective and radiant parts for both surfaces. Increase in δ leads to proportionally growing external heat source power required to heat the sample to the same temperature. It also requires testing time proportional to thickness squared for thermal wave to travel minimally required distance $\sim 10\delta$ to achieve the measurement accuracy of a few per cents employing the proposed cylinder wave model. It should be mentioned that for plates with $\delta \sim 1$ mm, both cylinder and spherical models may be used, though the former requires much higher testing time τ, while the latter requires higher spatial and temporal resolution from the camera and much better laser beam focusing.

Let us stress one more time that both described modes of the proposed approach do not require absolute values of surface temperature or heat fluxes, whereas neither data processing algorithms nor equation for determining a value do not require them. The only assumption of IR radiation value uniformity across the surface is enough. Possible optical inhomogeneities are suppressed significantly at the stage of pixel-by-pixel subtraction of the base image obtained before heating onset from every following image.

So that, the paper presents new express nondestructive testing technique for TPC measurement for both massive objects and thin plates including bulky components and elements of finished products, which does not require extensive sample preparation. Testing the technique ascertains that TD coefficient measured according to the proposed procedure coincides with known standard value or value measured by independent steady-state method with good accuracy.

The described approach can be considered as a further development of standard laser flash technique [14–17]. Low standard errors and low requirements for measurement conditions are mostly due to analysis of not just the only function $T(t)$ of one argument acquired just once per testing, but large two-dimensional array of data $T(r, t)$, while for each given value of t, the dependence $T(r)$ results from the averaging of tens to hundreds of points located at the same distance to the center of the heating spot. Recording spatial and temporal dynamics of thermal wave propagation allows averaging temperature data twice—firstly at r = const over the angle φ up to 0–360° range averaging several tens or even hundreds of pixels, and then over time by data analysis of several hundreds of individual frames of IR film.

In case of anisotropic materials of macroscopic inhomogeneities, averaging temperatures from pixels located at r = const can be done at $\varphi < 360°$ and then analyzed and plotted as $a(\varphi)$ or processing as usual just excluding the arcs where discrepancies exceed noise level by a given relative value. In the latter case, it can be an indication of material defects and could be a basis for developing highly sensitive differential techniques of thermographic nondestructive testing [68]. The region selected this way can be inspected in more detail on demand by changing the heating center position, or results of several tests for TD measurement using φ = 360° can be averaged to diminish inaccuracies further.

The main sources of systematic errors of the proposed technique are:

1. Thermographic techniques are affected by the scaling factor linking pixels and real length; for this reason, special care should be taken in the procedures for

determining actual geometrical factor. Additional inaccuracies can be brought about by errors in frame timestamps written by camera or personal computer running nonrealtime operating system.

2. Discrepancy with the model due to:

    a. incomplete suppression of optical inhomogeneities of the surface by image processing software,

    b. nonpoint-like heating especially in semitransparent material,

    c. stray and reflected light and IR-radiation, including that originating from laser beam collimation system; and

    d. imperfect abiding to adiabatic condition, i.e., significant convective or radiation heat flow across the surface.

6. Nondestructive testing using point heating

Thermographic approaches to nondestructive testing (T-NDT) seem promising for a wide variety of specific applications [3–7]. They can be multifunctional, multiscale, and contactless [20, 24, 35, 79–84]. Pulsed techniques have a number of advantages over quasi-stationary ones [20, 24, 69, 79, 80, 85] such as higher information content, higher spatial resolution, higher sensitivity to inhomogeneities, on the other hand, they require more powerful heat sources, higher resolution of data acquisition system, and more sophisticated thermal-physical models and data processing algorithms. It is convenient to create transient thermal fields by short-term heat supply to the area of interest. There are a lot of T-NDT techniques utilizing IR-cameras capable to resolve numerous issues concerning defect or suspicious sites detection and localization [6–8]. However, its potential has not been fully realized yet, and further advances in IR-cameras spatial and temporal resolution and data processing algorithms enable resolving more and more complex problems in monitoring and diagnostics.

We further describe the experimental and data processing techniques combining crack detection, localization, and characterization with enhanced signal-to-noise ratio and sensitivity to small defects.

6.1 Stepwise point heating technique for NDT

The technique is based upon computer analysis of transient thermal field generated by an external heat source localized at the spot with 0.1–0.3 mm radius [85]. Such a source produces radially symmetric heat wave in a defect-free plate, so that the position of concentric isotherms at any time can be obtained with high accuracy by averaging signals from a large number of IR-camera pixels at r = const as described in the first part of the paper. A defect locally contorts the isotherm circular shape, making it a good diagnostic indicator. The technique is differential at the root that provides high sensitivity and signal/noise ratio of the testing.

A number of model defects, namely part-through notches made on either front or rear sides of the metal plates by a thin (0.8 mm) abrasive microdisk, have been studied experimentally. These tests give temperature distributions related to typical defects and allow evaluation of the developed model and software adequacy for thermal image analysis. To reduce camera matrix random noise, the signal from

every pixel has been averaged over 10–60 sequential frames. The experiments have been carried out on the plate with 3-mm thickness made of mild carbon steel "Steel 40X" (analog of mild carbon steel AISI 5140).

6.2 NDT results

As can be seen in **Figure 1** presenting typical raw data, experimentally obtained isotherms at a defect-free plate can be approximated with concentric circles with high accuracy. A defect distorts circular shape of isotherms locally. Thus, **Figure 8** demonstrates an instance of the temperature field in an area containing part-through notch with length L = 15 mm and depth h = 2.5 mm at the rear side of the plate. Isotherms distortion induced by the notch is quite specific. They swell outward from the center at the cut bank facing the heating center and inward at the opposite bank (see **Figure 8b**). The above distortion is due to the additional thermal resistance introduced by the notch to the thermal flow, so that the temperature at the notch side facing the heat source goes slightly up relative to the defect-free area at the same distance from the heat source, while the temperature at the other side goes slightly down.

The data discussed above comprise an input for further processing. Subtraction of temperature TR averaged over angle φ over the defect-free region from the T allows detecting temperature field variations ΔT_d, originating from much smaller defects than could be seen by the naked eye. **Figure 9** presents distributions of differential temperature ΔT_d at the surface in two perpendicular directions along and across the plane of the part-through notch with length L = 15 mm and depth h = 2.5 mm on the hidden side of the plate. The maximal temperature difference ΔT_{max} between the points with the highest and the lowest ΔT_d in the region around the notch depends on its length, depth, angle φ between its axis and direction to the heating center (**Figure 10a**) and distance to it (**Figure 10b**). At the most favorable circumstances, this technique is capable to detect and characterize notches with length L around a few millimeters at the signal to noise ratio 3:1. Weak ΔT_{max} dependence on angle φ provided $\varphi > 10°$ and rather wide range of distances R between the defect and the heating center where the distance dependence is also weak allows one to detect and characterize multiple cracks with unknown position and orientation in a certain region in a single test.
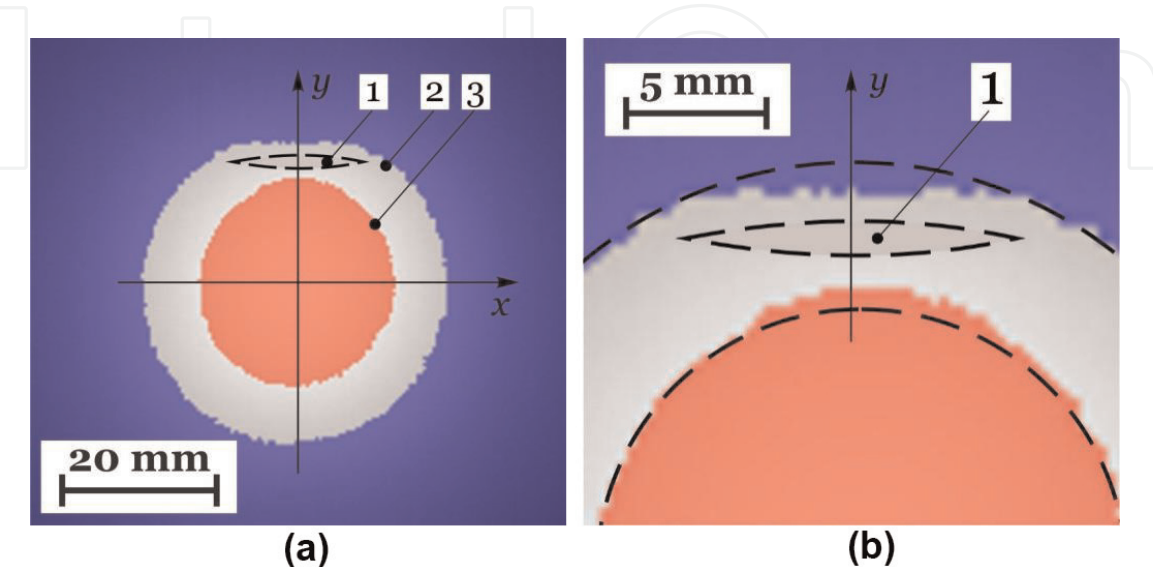

(a)   **(b)**

Figure 8.
Typical temperature distribution resulting from local heating of the steel plate containing part-through notch with L = 15 mm and depth h = 2.5 mm during 60 s in different scales (a) and (b) with superimposed isotherms. 1—notch, 2—T = 15°C, 3—T = 20°C.
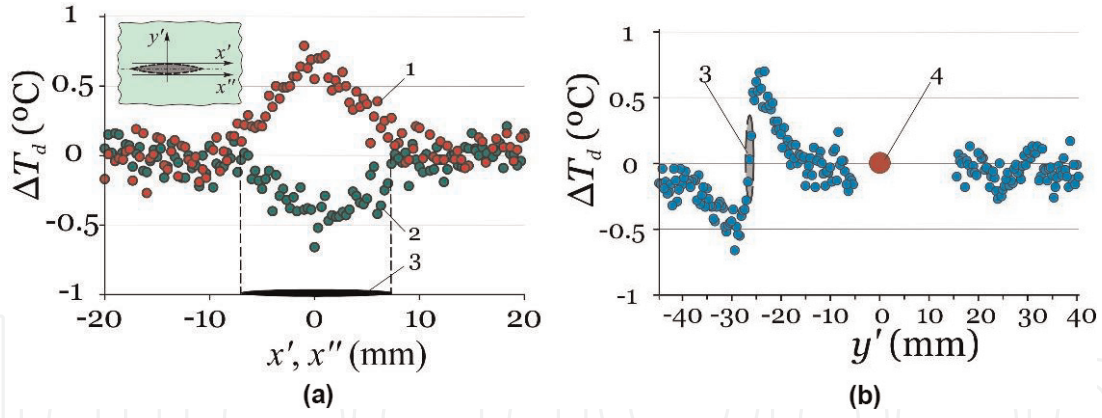
Figure 9.
Temperature profiles along x' and x axes (a) and along y' axis (b) after 60 s of local heating at zero point of the steel plate containing 15-mm-length part-through notch at the hidden side. 1—in front of the notch, 2—behind the notch, 3—notch position, 4—heating center, and ΔT_d—temperature difference.
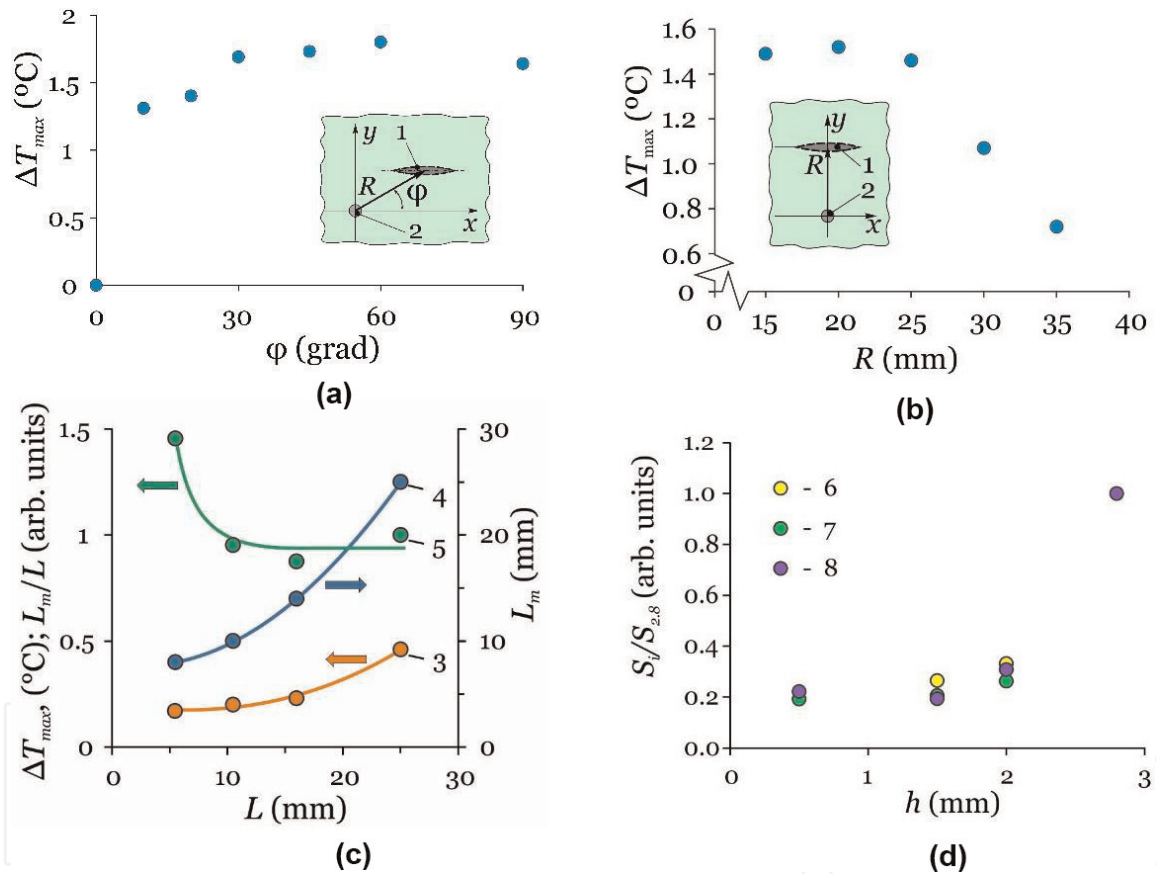

Figure 10.
Experimentally found dependences of values related to part-through notches on the hidden side of the plate. (a) ΔT_{max} over the angle φ between the notch plane and radius-vector R from the heating center to the notch center as shown in the inset (1—notch and 2—heating center); (b) ΔT_{max} over the distance R; (c) 3—ΔT_{max}, 4—width of ΔT_d profile raise L_m, and 5—L_m/L ratio over the notch length L; (d) signal ratio $S_i(h)/S_i(2.8)$ at different data processing iterations (6—S_0; 7—S_3; and 8—S_{4d}) over the notch depth h. ΔT_{max} is maximal temperature difference at the region near the notch.

The width of the raise in ΔT_d distribution along the notch is well correlated with the notch length L (see **Figure 10c**). So, it is a convenient value to characterize the length L, and the experiment results (see **Figure 10c**) prove that starting from several millimeters, the length L can be determined with the accuracy better than 10%. The maximum of the distribution ΔT_{max} weakly depends upon the notch length and cannot be used as a reliable indicator. ΔT_{max} dependence upon the notch depth h is prominently nonlinear, and for shallow notches with depth up to 2/3 of

plate thickness, it is quite weak too (see **Figure 10d**). It does not allow reliable determination of the depth of such defects.

6.3 Shallow notch detection enhancing

The signal originated from the notch is obscured by noise for $h < 0.5\,\delta_m$ where δ_m is the plate thickness, so that it is very difficult not only to evaluate the notch depth from raw signal, but even to detect its presence. To detect such defects producing low-amplitude short-range deviations of a specific pattern in the temperature field, it is possible to use gradient methods with a large window with the size smaller but comparable to the characteristic defect fingerprint extension. So we propose the following procedure: for every pixel, the absolute value of temperature gradient is calculated at quite a large window like 9×9 or 13×13 pixels that is about 3×3 or 4×4 mm, producing a slope map of the original image. It reduces noise drastically and enhances field irregularities with the characteristic size about that of the window. This operation is then repeated several times in diminishing windows, so that the slope image of the slope image, etc. is calculated, which are further referred to as $S_{i+1} = |\text{grad } S_i|$ where i is the iteration number. Successive iterations do not significantly affect the ratio of signals produced by the notches of different depth as shown in **Table 3** and **Figure 10d**, but notably improve signal/noise ratio, thus enhancing our capability to detect shallow notch as shown in **Table 4** and **Figure 11**. Additional way to improve signal/noise ratio is to obtain the differences $S_{id} = \partial S_i / \partial x$ between adjacent points of S_i along the line perpendicular to the notch. Thus, preliminary detection technique can be based upon a local exceedance of some threshold value of S_i, followed by confirmation using S_{id} level.

The result of four successive computations of gradient absolute values S_1–S_4 over the full image is shown in **Figure 11** at the lines perpendicular to the notches along with S_{4d}, which is a signed uniaxial derivative of S_4 along the selected line. As could be seen, the notch with $h = 0.5$ mm located at $x = 20$ mm can be reliably detected by signal level from the third iteration on. **Table 4** presents signals from notches with varying depths normalized to the signal of notch with $h = 2.8$ mm, at various processing stages. S_0 is the raw signal averaged in 5×5 pixel window. **Table 2** presents signal/noise ratios for two notches with length $L = 15$ mm and depths of 0.5

h (mm)	Iteration							
	S_0	S_1	S_2	S_{2d}	S_3	S_{3d}	S_4	S_{4d}
0.5	0.22	0.20	0.19	0.24	0.19	0.22	0.22	0.22
1.5	0.26	0.24	0.20	0.30	0.20	0.23	0.20	0.19
2.0	0.33	0.29	0.27	0.32	0.26	0.35	0.28	0.31

Table 3.
Dependence of sensitivity to crack depth h *as* $S_i(h)/S_i(2.8)$ *upon signal processing method.*

h (mm)	Iteration							
	S_0	S_1	S_2	S_{2d}	S_3	S_{3d}	S_4	S_{4d}
0.5	0.51	1.16	1.69	2.15	1.88	2.38	2.40	3.10
2.8	2.36	5.77	9.03	8.93	9.76	10.6	11.0	14.0

Table 4.
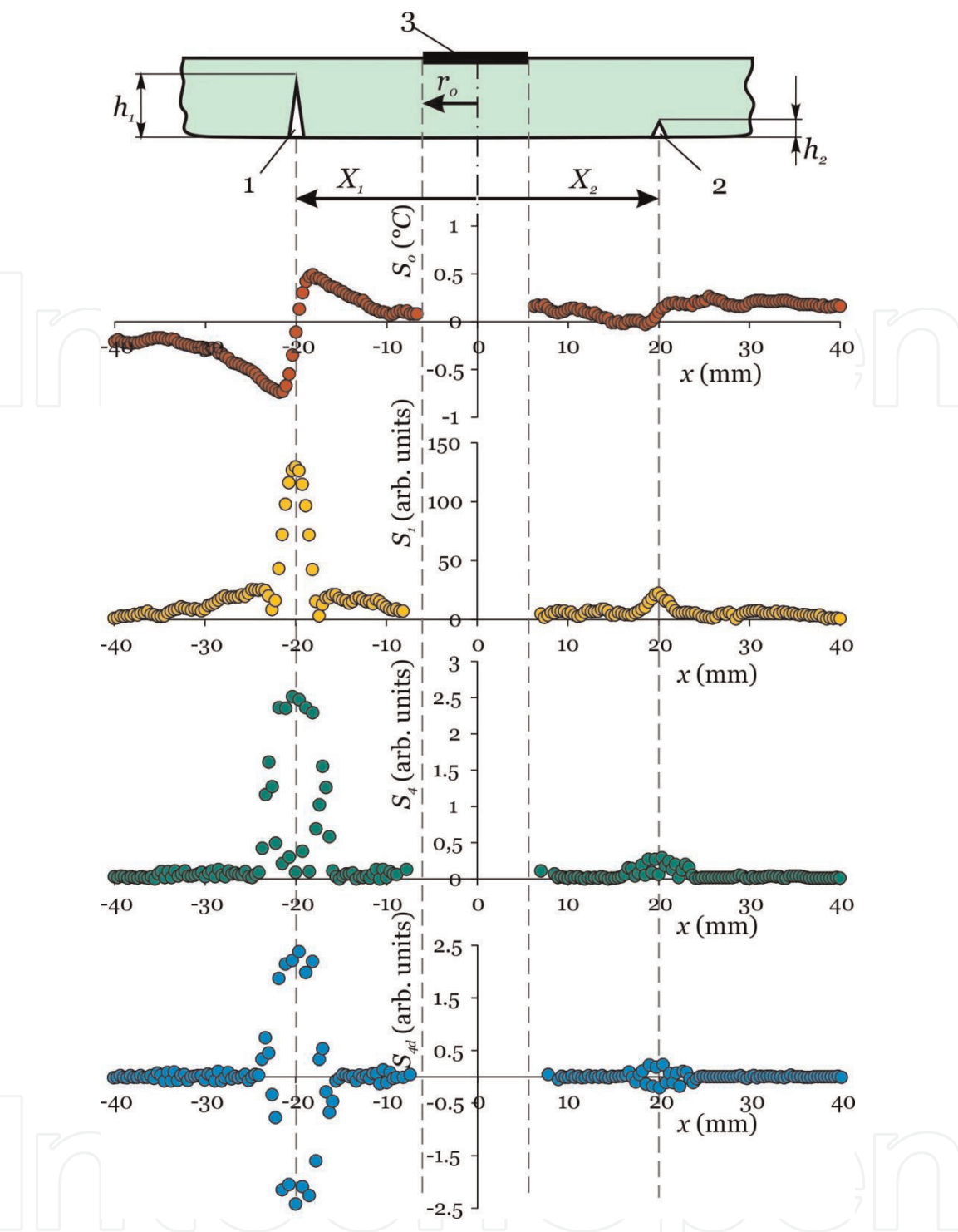*Dependence of signal/noise ratio for two cracks upon signal processing method.*

Figure 11.
Profiles of the signal at different stages of data processing along the x axis. S_o is raw temperature T averaged over 1.5×1.5 mm^2 area, i.e., 5×5 pixels. The heating region is marked by the dashed lines. $S_1 = |grad\ T|$, $S_4 = |grad\ S_3|$, $S_{4d} = \partial S_4/\partial x$. Inset schematically presents experiment layout. Notches h_1 (1) and h_2 (2) ($h_1 > h_2$) and heating region (3).

and 2.8 mm at the same processing stages. Both signal and noise values in the tables refer to the peak values.

7. Conclusions

Let us briefly summarize the most important characteristic features and main advantages of the proposed technique justified by the experimental results:

1. The proposed technique is adequate within a wide time range providing several hundreds of individual values of *a* differing by no more than 10–15% to obtain the averaged result from the film. Moreover, each individual measurement results from processing temperature distribution obtained, in turn, by averaging large number of pixels located at the same distance from the heating center. Such double averaging results in very low random error, which is around a few per cent and supplies rich statistics providing quite accurate measurements. The best results were obtained on testing stabilized zirconia ceramics, which has the most uniform optical properties and microstructure of all tested materials. Relative random error of TD measured in single test was below 2% for this material.

2. Short duration τ of the testing—for the tested materials with moderate values of $a \sim 0.1$–15 mm^2/s, τ = 3–20 s. τ decreases with growing *a* and better heating localization.

3. Continuous heating during several seconds of testing as opposed to "instant" heating by very high peak intensity pulse in LFT excludes severe overheating of sample material. At any time and for all materials, maximal overheatings in the heating spot and in the measurement area do not exceed several tens and several kelvins accordingly. For the vast majority of cases, it allows neglecting the effect of temperature dependence of temperature diffusivity on obtained value.

4. Consequently, low duration τ leads to diminishing inaccuracies originated from heat losses across the surfaces, contributions from surrounding constructions, drifts, and others.

5. Loose requirements for sample preprocessing and geometry—minimal 3D sample dimensions are 5–10 mm in any direction from the heating center, and the surface in this area should be macroscopically flat, namely surface roughness should not exceed 20–50 mkm. Higher roughness values result in increasing measurement random errors, but short testing duration makes statistics collection easy. Corrections for surface curvature can be introduced if necessary.

6. Weak dependence or almost complete independence of surface optical properties impact on the measurement results apart from transparent materials with low factors of volume absorption and stray light.

7. Good results reproducibility with TD root mean square in order of a few per cent.

8. Testing is still possible if only one side of the tested object is freely available.

9. Technical plausibility of designing inexpensive portable device for express testing various objects including large sized ones. Due to its simplicity and high testing rate, it can be installed in production lines for *in situ* quality control or used for out-of-the-laboratory control of finished products quality.

10. Dynamic thermographic technique has been developed for testing shells, plates, vessels, tubes, reactors, fuselage elements, etc. It is capable of detecting defects with length above a few millimeters and depth more than a

few tenths of millimeters not only at the visible but also at the inner unreachable side of the shell.

Acknowledgements

Conflicts of interest

The authors declare no conflict of interest.

Author details

Dmitry Yu. Golovin[1], Alexander G. Divin[2], Alexander A. Samodurov[1], Alexander I. Tyurin[1] and Yuri I. Golovin[1,3*]

1 Research Institute for Nanotechnologies and Nanomaterials, Derzhavin Tambov State University, Tambov, Russia

2 Tambov State Technical University, Tambov, Russia

3 Chemical Department, Lomonosov Moscow State University, Moscow, Russia

*Address all correspondence to: yugolovin@yandex.ru

IntechOpen

References

[1] Vavilov VP. Thermal NDT: Historical milestones, state-of-the-art and trends. Quantitative InfraRed Thermography Journal. 2014;**11**:66-83

[2] Hudson RD. Infrared System Engineering. New York (NY): Wiley-Interscience; 1969. p. 672

[3] Haddadnia J, Zadeh HG. The New Trends in the Application of Thermography Science for Diagnostic Purposes. Reseda, CA, USA: Supreme Century; 2016. p. 152

[4] Gaussorgues G, Chomet S. Infrared Thermography. Netherlands: Springer Science and Business Media; 2012. p. 508

[5] Vollmer M, Möllmann K-P. Infrared Thermal Imaging: Fundamentals, Research and Applications. Wiley-VCH: Weinheim; 2010. p. 612

[6] Meola C, Ibarra-Castanedo C, Maldague XPV. Infrared Thermography Recent Advances and Future Trends (Bentham eBooks). 2012Infrared thermography. In: Czichos H, editor. Handbook of Technical Diagnostics. Berlin, Heidelberg: Springer-Verlag; 2013. pp. 175-220

[7] Usamentiaga R, Venegas P, Guerediaga J, Vega L, Molleda J, Bulnes FG. Infrared thermography for temperature measurement and non-destructive testing. Sensors. 2014;**14**: 12305-12348

[8] Ciampa F, Mahmoodi P, Pinto F, Meo M. Recent advances in active infrared thermography for non-destructive testing of aerospace components. Sensors. 2018; **18**:609-646

[9] Prakash RM. Infrared Thermography. Rijeka, Croatia: InTech; 2012. p. 245

[10] Breitenstein O, Warta W, Langenkamp M. Lock-in Thermography: Basics and Use for Evaluating Electronic Devices and Materials. New York: Springer; 2010. p. 257

[11] Bar-Cohen A, Matin K, Narumanchi S. Nanothermal interface materials: Technology review and recent results. Journal of Electronic Packaging. 2015; **137**:040803-1-040803-17

[12] Choudhary A, Goyal D, Shimy SL, Akula A. Condition monitoring and fault diagnosis of induction motors: A review. Archives of Computational Methods in Engineering. 2018:1-18. Available from: https://doi.org/10.1007/s11831-018-9286-z

[13] Xingwang G, Vavilov VP. Pulsed thermographic evaluation of disbonds in the insulation of solid rocket motors made of elastomers. Polymer Testing. 2015;**45**:31-40

[14] Subramainam B, Lahiri BB, Saravanan T, Philip J. Infrared thermography for condition monitoring —A review. Infrared Physics and Technology. 2013;**60**:35-55

[15] Zhang H, Yang R, He Y, Foudazi A, Cheng L, Tian G. A review of microwave thermography nondestructive testing and evaluation. Sensors. 2017;**17**:1123-1156

[16] Kordatos EZ, Exarchos DA, Stavrakos C, Moropoulou A, Matikas TE. Infrared thermographic inspection of murals and characterization of degradation in historic monuments. Construction and Building Materials. 2013;**48**:1261-1265

[17] Theodorakeas P, Cheilakou E, Ftikou E, Koui M. Passive and active infrared thermography: An overview of applications for the inspection of mosaic

structures. Journal of Physics: Conference Series. 2015;**655**:012061

[18] Garrido I, Lagüela S, Arias P. Infrared thermography's application to infrastructure inspections. Infrastructures. 2018;**35**:1-19

[19] Lucchi E. Applications of the infrared thermography in the energy audit of buildings: A review. Renewable and Sustainable Energy Reviews. 2018;**82**:3077-3090

[20] Vavilov VP, Burleigh DD. Review of pulsed thermal NDT: Physical principles, theory and data processing. NDT&E International. 2015;**73**:28-52

[21] Balageas D, Maldague XD, Burleigh D, Vavilov VP, Oswald-Tranta JM, Roche B, et al. Thermal (IR) and other NDT techniques for improved material inspection. Journal of Nondestructive Evaluation. 2016;**35**:1-17

[22] Ibarra-Castanedo C, Tarpani JR, Maldague XPV. Nondestructive testing with thermography. European Journal of Physics. 2013;**34**:S91-S109

[23] Vavilov VP. Thermal nondestructive testing of materials and products: A review. Russian Journal of Nondestructive Testing. 2017;**53**:707-730

[24] Vavilov VP. Dynamic thermal tomography: Recent improvements and applications. NDT&E International. 2015;**71**:23-32

[25] Yang R, He Y. Optically and non-optically excited thermography for composites: A review. Infrared Physics and Technology. 2016;**75**:26-50

[26] Zhao Y, Addepalli S, Sirikham A, Roy R. A confidence map based damage assessment approach using pulsed thermographic inspection. NDT and E International. 2018;**93**:86-97

[27] Bodnar JL. Crack detection by stimulated infrared thermography. European Physical Journal Applied Physics. 2014;**65**:31001-31012

[28] Yüksel N. Chapter 6: Insulation materials in context of sustainability. In: Almusaed A, Almssad A, editors. The Review of Some Commonly Used Methods and Techniques to Measure the Thermal Conductivity of Insulation Materials. InTech; 2016. pp. 113-140

[29] Cernuschi F, Bison PG, Figari A, Marinetti S, Grinzato E. Thermal diffusivity measurements by photothermal and thermographic techniques. International Journal of Thermophysics. 2004;**25**:439-457

[30] Abad B, Borca-Tasciuc D-A, Martin-Gonzalez MS. Non-contact methods for thermal properties measurement. Renewable and Sustainable Energy Reviews. 2017;**76**:1348-1370

[31] Hammerschmidt U, Hameury J, Strnad R, Turzó-Andras E, Wu J. Critical review of industrial techniques for thermal-conductivity measurements of thermal insulation materials. International Journal of Thermophysics. 2015;**36**:1530-1544

[32] Doshvarpassand S, Wu C, Wang X. An overview of corrosion defect characterization using active infrared thermography. Infrared Physics and Technology. 2019;**96**:366-389

[33] Vostikolaei FS, Akhoondzadeh M. A comparison of four methods for extracting land surface emissivity and temperature in the thermal infrared hyperspectral data. Earth Observation and Geomatics Engineering. 2018;**2**:56-63

[34] Pereira CB, Yu X, Dahlmanns S, Blazek V, Leonhardt S, Teichmann D. Chapter 1: Infrared thermography. In: Abreu de Souza M et al., editors. Multi-

Modality Imaging. Switzerland AG: Springer Nature; 2018. pp. 1-29

[35] Lahiri BB, Bagavathiappan S, Jayakumar T, Philip J. Medical applications of infrared thermography: A review. Infrared Physics and Technology. 2012;**55**:221-235

[36] JIP Q. Application of Infrared Thermography in Sports Science. Switzerland: Springer; 2017. p. 339

[37] Zhao D, Qian X, Gu X, Jajja SA, Yang R. Measurement techniques for thermal conductivity and interfacial thermal conductance of bulk and thin film materials. Journal of Electronic Packaging. 2016;**138**:040802-1-040802-19

[38] Okamoto Y, Watanabe S, Ogata K, Hiramatsu K, Miyazaki H, Morimoto J. Proposal of novel measurement method for thermal diffusivity from infrared thermal movie. Japanese Journal of Applied Physics. 2017;**56**:056601

[39] Tailor RE, Maglik KD. Pulse method for thermal diffusivity measurement, compendium of thermophysical property measurement methods. In: Maglic KD et al., editors. Survey of Measurement Techniques. Vol. 1. New York: Plenum Press; 1984. pp. 305-336

[40] Chernuschi F, Figari A, Fabbri L. Thermal wave interferometry for measuring the thermal diffusivity of thin slabs. Journal of Materials Science. 2000;**35**:5891-5897

[41] Parker WJ, Jenkins RJ, Butler CP, Abbot GL. Flash method of determining thermal diffusivity, heat capacity and thermal conductivity. Journal of Applied Physics. 1961;**32**:1679-1684

[42] Vozar L, Hohenauer W. Flash method of measuring the thermal diffusivity. A review. High Temperatures - High Pressures. 2003/2004;**35/36**:253-264

[43] McMasters RL, Dinwiddie RB. Anisotropic thermal diffusivity measurement using the flash method. Journal of Thermophysics and Heat Transfer. 2014;**28**:518-523

[44] Kruczek T, Adamczyk WP, Bialecki RA. In situ measurement of thermal diffusivity in anisotropic media. International Journal of Thermophysics. 2013;**34**:467-485

[45] Wang L, Gandorfer M, Selvam T, Schwieger W. Determination of faujasite-type zeolite thermal conductivity from measurements on porous composites by laser flash method. Materials Letters. 2018;**221**:322-325

[46] Salazar A, Mendioroz A, Apiñaniz E, Pradere C, Noël F, Batsale J-C. Extending the flash method to measure the thermal diffusivity of semitransparent solids. Measurement Science and Technology. 2014;**25**:035604

[47] Coquard R, Panel B. Adaptation of the flash method to the measurement of the thermal conductivity of liquids or pasty materials. International Journal of Thermal Sciences. 2009;**48**:747-760

[48] Shao X, Mo S, Chen Y, Yin T, Yang Z, Jia L, et al. Solidification behavior of hybrid TiO_2 nanofluids containing nanotubes and nanoplatelets for cold thermal energy storage. Applied Thermal Engineering. 2017;**117**:427-436

[49] Noroozi M, Zakaria A. Chapter 4: Measuring nanofluid thermal diffusivity and thermal effusivity: The reliability of the photopyroelectric technique. In: Nanofluid Heat and Mass Transfer in Engineering Problems. Intech; 2017. pp. 65-93

[50] Azmi W, Sharma K, Mamat R, Najafi G, Mohamad M. The enhancement of effective thermal conductivity and effective dynamic

viscosity of nanofluids—A review. Renewable and Sustainable Energy Reviews. 2016;**53**:1046-1058

[51] Murshed S, De Castro C. Superior thermal features of carbon nanotubesbased nanofluids—A review. Renewable and Sustainable Energy Reviews. 2014;**37**:155-167

[52] Tertsinidou G, Tsolakidou C, Pantzali M, Assael M. New measurements of the apparent thermal conductivity of nanofluids and investigation of their heat transfer capabilities. Journal of Chemical and Engineering Data. 2017;**62**:491-507

[53] Laser Flash Analysis—LFA. Method, Technique, Applications. NETZSCH-Geratebau GmbH [Internet]. 2019. Available from: http://www.netzsch.com [Accessed: 11 June 2019]

[54] Discovery Flash. [Internet]. 2019. Available from: https://www.tainstruments.com [Accessed: 11 June 2019]

[55] ISO 22007-4. Plastics—Determination of thermal conductivity and thermal diffusivity—Part 4: Laser flash method; 2017

[56] ISO 18755. Fine ceramics (advanced ceramics, advanced technical ceramics). Determination of thermal diffusivity of monolithic ceramics by laser flash method; 2005

[57] ASTM E1461-13. Standard test method for thermal diffusivity by the flash method

[58] Donaldson AB, Taylor RE. Thermal diffusivity measurement by a radial heat flow method. Journal of Applied Physics. 1975;**46**:4584-4589

[59] Cernuschi F, Russo A, Lorenzoni L, Figari A. In-plane thermal diffusivity evaluation by infrared thermography. Review of Scientific Instruments. 2001;**72**:3988-3995

[60] Dong H, Zheng B, Chen F. Infrared sequence transformation technique for in situ measurement of thermal diffusivity and monitoring of thermal diffusion. Infrared Physics and Technology. 2015;**73**:130-140

[61] Genna S, Ucciardello N. A thermographic technique for in-plane thermal diffusivity measurement of electroplated coatings. Optics and Laser Technology. 2019;**113**:338-344

[62] Bedoya A, González J, Rodríguez-Aseguinolaza J, Mendioroz A, Sommier A, Batsale JC, et al. Measurement of in-plane thermal diffusivity of solids moving at constant velocity using laser spot infrared thermography. Measurement. 2019;**134**:519-526

[63] Cielo P, Utracki LA, Lamontagne M. Thermal diffusivity measurements by the converging-thermal-wave technique. Canadian Journal of Physics. 1986;**64**:1172-1177

[64] Murphy F, Kehoe T, Pietralla M, Winfield R, Floyd L. Development of an algorithm to extract thermal diffusivity for the radial converging wave technique. International Journal of Heat and Mass Transfer. 2005;**48**:395-402

[65] Kehoe T, Murphy F, Kelly P. A method for measuring the thermal diffusivity of intermediate thickness surface absorbing samples and obtaining the ratio of anisotropy by the converging wave flash method. International Journal of Thermophysics. 2009;**30**:987-1000

[66] Kim SW, Kim JC, Lee SH. Analysis of thermal diffusivity by parameter estimation in converging thermal-wave technique. International Journal of Heat and Mass Transfer. 2006;**49**:611-616

[67] Husin MS, Moksin MM, Jibrin S, Azmi BZ, Yunus WMM, Waziri M. A simplified low cost converging thermal wave technique for measuring thermal

diffusivity of thin foils. IOSR Journal of Applied Physics. 2013;**3**:38-46

[68] Golovin YI, Turin AI, Golovin DY, Samodurov AA. New methods of thermographic control using multi-scale analysis of non-stationary thermal fields. Industrial Laboratory (Diagnostics of Materials). 2018;**84**: 23-33

[69] Almond DP, Angioni SL, Pickering SG. Long pulse excitation thermographic non-destructive evaluation. NDT&E International. 2017; **87**:7-14

[70] Badghaish AA, Fleming DC. Non-destructive inspection of composites using step heating thermography. Journal of Composite Materials. 2008; **42**:1337-1357

[71] Roche J-M, Balageas D. Common tools for quantitative pulse and step-heating thermography—Parts l and ll. QIRT Conference; Bordeaux, France; 2014. pp. 1-28

[72] Palumbo D, Cavallo P, Galietti U. An investigation of the stepped thermography technique for defects evaluation in GFRP materials. NDT and E International. 2019;**102**: 254-263

[73] Carslaw HC, Jaeger JC. Conduction of Heat in Solids. Vol. 510. USA: Oxford University Press; 1959

[74] Babichev AP, Babushkina NA, Bratkovskii AM, et al. In: Grigoriev IS, Melikhova EZ, editors. Handbook on Physical Quantities. Moscow: EnergoAtomIzdat; 1991. p. 1232. (in Russian)

[75] Watanabe H. Further examination of the transient hot-wire method for the simultaneous measurement of thermal conductivity and thermal diffusivity. Metrologia. 2002; **39**:65-81

[76] Merckx B, Dudoignon P, Garnier JP, Marchand D. Simplified transient hot-wire method for effective thermal conductivity measurement in geo materials: Microstructure and saturation effect. Advances in Civil Engineering. 2012;**2012**:1-10

[77] Assael MJ, Dix M, Gialou K, Vozar L, Wakeham WA. Application of the transient hot-wire technique to the measurement of the thermal conductivity of solids. International Journal of Thermophysics. 2002;**23**: 615-633

[78] Guo W, Li G, Zheng Y, Dong C. Measurement of the thermal conductivity of SiO_2 nanofluids with an optimized transient hot wire method. Thermochimica Acta. 2018;**661**:84-97

[79] Assael MJ, Antoniadis KD, Wakeham WA. Historical evolution of the transient hot-wire technique. International Journal of Thermophysics. 2010;**31**:1051-1072

[80] Liang K, Ma Y, Xie Y, Zhou B, Wang R. A new adaptive contrast enhancement algorithm for infrared images based on double plateaus histogram equalization. Infrared Physics and Technology. 2012;**55**:309-315

[81] Gao B, Woo WL, Tian GY. Electromagnetic thermography nondestructive evaluation: Physics-based modeling and pattern mining. Scientific Reports. 2016;**6**:25480

[82] Qiu J, Pei C, Liu H, Chen Z, Demachi K. Remote inspection of surface cracks in metallic structures with fiber-guided laser array spots thermography. NDT and E International. 2017;**92**:213-220

[83] Xu C, Gong X, Xumei X, Zhang W, Chen G. An investigation on eddy current pulsed thermography to detect surface cracks on the tungsten carbide matrix of polycrystalline diamond

compact bit. Applied Sciences. 2017;7: 1-12

[84] Tavakolian P, Sivagurunathan K, Mandelis A. Enhanced truncated-correlation photothermal coherence tomography with application to deep subsurface defect imaging and 3-dimensional reconstructions. Journal of Applied Physics, 2017;**122**:023103–1–023103–10

[85] Golovin YI, Tyurin AA, Golovin DY, Samodurov AA. Radially-symmetric thermal wave as a source of information on the state of ingomogenity in plates and sheaths. Russian Physics Journal. 2018;**61**:1472-1477